Advanced AUV Motion Control and Terrain Following for Automatic Seabed Inspection

Università di Genova

Fabio Guelfi

DIBRIS - Department of Computer Science, Bioengineering, Robotics and System Engineering

University of Genova

Supervisors:
Prof. Enrico Simetti
Prof. Antonio Pascoal

In partial fulfillment of the requirements for the degree of

Laurea Magistrale in Robotics Engineering

October 14, 2025

Declaration of Originality

I, Fabio Guelfi, hereby declare that this thesis is my own work and all sources of information and ideas have been acknowledged appropriately. This work has not been submitted for any other degree or academic qualification. I understand that any act of plagiarism, reproduction, or use of the whole or any part of this thesis without proper acknowledgment may result in severe academic penalties.

Acknowledgements

This is an optional section, where you can write acknowledgments. Don't forget to acknowledge your supervisor!

This is a short, optional, dedication. To all the Master and PhD students of Robotics Engineering at the University of Genova.

Abstract

The abstract should be a concise report of what the thesis is about. Do not use citations here, and avoid the use of abbreviations. It should not exceed one page of length.

Contents

List of Figures

Chapter 1

Introduction

1.1 Content

In the introduction, please state clearly the context your work is framed within, and the motivations of your work. Furthermore, it is important to clarify your contribution (and not those of the group you work in - it is still an exam after all). Provide an outline of the thesis.

1.2 Basic commands

This is a citation: Caccia *et al.* (1999). Make sure to correctly enter all the bibliographic details. It is important that you double check them when retrieving the bibtex file from a source such as Google Scholar. Consistency in the references is valued by the Committee.

This is an emphasized word: *global*.
This is a reference to another part of the thesis: Chapter 2.
This is an enumerated list:

1. first item.
2. second item.

This is an in-line equation: $x-$.
This is a word in quotes: "regular".

1.3 Equation

This is an equation:

$$\mathcal{U}_k(s_k) = \frac{P_k}{C_k}. \tag{1.1}$$

Equations follow the punctuation rules, as if they were inline with the text. This is an equation split over multiple lines:

$$\begin{aligned} x_k &= \mathcal{F}(x_{k-1}, u_k, w_{k-1}), \\ z_k &= \mathcal{H}(x_k, v_k). \end{aligned} \tag{1.2}$$

This is an example of equation with matrices:

$$\mathcal{Q}_l = \frac{d_l^2 \sigma_\phi^2}{2} \begin{bmatrix} 2\sin^2\phi_l & -\sin 2\phi_l \\ -\sin 2\phi_l & 2\cos^2\phi_l \end{bmatrix} \begin{bmatrix} cc\frac{\sigma_d^2}{2} & 2\cos^2\phi_l & \sin 2\phi_l \\ & \sin 2\phi_l & 2\sin^2\phi_l \end{bmatrix}. \tag{1.3}$$

This is a reference to the Equation 1.2. Avoid using unnumbered equations as it makes it difficult to reference them during a discussion. Also, be consistent in the use of matrix or vector notation. For example, $\dot{\boldsymbol{x}} = \boldsymbol{A}\boldsymbol{x} + \boldsymbol{B}\boldsymbol{u}$ or $\boldsymbol{y} = \alpha\boldsymbol{x}$, where the α is a scalar. You can change the corresponding definitions in the class file, as long as you remain consistent.

1.4 Figure

I add a figure.

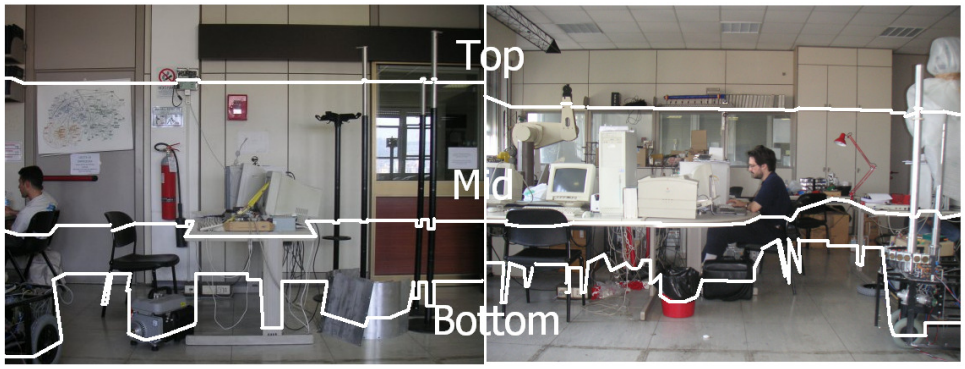

Figure 1.1: Scan profiles: *bottom*, *mid* and *top view*.

Make sure that figures axis are readable. Make sure to label all the units on both axes. The width of the lines should be also crosschecked for readability (the typical MATLAB plot might need higher line width). Double check that legends are present. Figures' captions should allow the reader to fully understand the figure.

This is a reference to Figure 1.1.

1.5 Table

The suggested packages for tables is tabular. There are many examples on the Internet. In general, avoid vertical lines, and use horizontal lines sparingly. Here S allows to align to the decimal point.

m	$\Re\{\underline{\mathfrak{X}}(m)\}$	$-\Im\{\underline{\mathfrak{X}}(m)\}$	$\mathfrak{X}(m)$	$\frac{\mathfrak{X}(m)}{23}$	A_m	$\varphi(m)$ / °	φ_m / °
1	16.128	8.872	16.128	1.402	1.373	−146.6	−137.6
2	3.442	−2.509	3.442	0.299	0.343	133.2	152.4
3	1.826	−0.363	1.826	0.159	0.119	168.5	−161.1
4	0.993	−0.429	0.993	0.086	0.08	25.6	90
5	1.29	0.099	1.29	0.112	0.097	−175.6	−114.7
6	0.483	−0.183	0.483	0.042	0.063	22.3	122.5
7	0.766	−0.475	0.766	0.067	0.039	141.6	−122
8	0.624	0.365	0.624	0.054	0.04	−35.7	90
9	0.641	−0.466	0.641	0.056	0.045	133.3	−106.3
10	0.45	0.421	0.45	0.039	0.034	−69.4	110.9
11	0.598	−0.597	0.598	0.052	0.025	92.3	−109.3

1.6 Algorithm

This is an algorithm:

Algorithm 1 Split & Merge [& Split]

Require: A scan s. A stack $\mathcal{L}$. A counter j. A threshold τ
Ensure: $\lambda \leftarrow \mathcal{M}(s)$, $j = 1, ..., |\lambda|$

$\mathcal{L} = \texttt{push}(s)$
$j \leftarrow 1$
while $\mathcal{L} \neq \varnothing$ **do**
  $\mathcal{L} = \texttt{pop}(s_{top})$
  $l_j \leftarrow \texttt{fitting}(s_{top})$
  $q_k = \text{argmax}_q \, \texttt{dist(l}_j\texttt{,q)}$
  if $\texttt{dist(l}_j\texttt{,}q_k\texttt{)} < \tau$ **then**
    $j \leftarrow j + 1$
    `continue`
  else
    $s_a \leftarrow \texttt{sub}(s_{top}, 1, k)$
    $s_b \leftarrow \texttt{sub}(s_{top}, k + 1, |s|)$
    $\mathcal{L} = \texttt{push}(s_a)$
    $\mathcal{L} = \texttt{push}(s_b)$
  end if
end while
$\{l_j\} \leftarrow \texttt{merge}(\{l_j\})$
$\{l_j\} \leftarrow \texttt{split}(\{l_j\})$

1.7 Historical background

The first real underwater explorations date back to the Phoenicians, Greeks, and Romans, who, through diving and free diving, recovered corals, sponges, and objects from the seabed, in addition to defenses Erodoto (V sec. a.C.). Many years later, in 1535, Guglielmo de Lorena designed the first underwater bell for underwater inspections, but only at shallow depths Eliav (2015). It was not until 1934 that the first real exploratory expedition took place with William Beebe and Otis Barton's bathyscaphe to a depth of about 923 meters, and in 1960, Auguste Piccard's bathyscaphe, the Trieste, reached a depth of 10,916 meters in the Mariana Trench Jacques Piccard (1961).

1.7.1 Marine robotics

With the advent of technology, remotely operated vehicles (ROVs) emerged, allowing for deeper and more complex underwater exploration without putting human divers at risk. The most complex challenge was the communication between the

ROV and the surface vessels. The solution was to build tethered systems that could maintain a constant connection. The CURV, Cable Controlled Undersea Recovery Vehicle, was the first ROV to be used in underwater missions.

1.7.2 Autonomous navigation

1.7.3 Underwater mission in seabed inspection

1.8 Motivation

1.9 Problem statement

1.10 Previous work and main contribution

1.10.1 Terrain tracking types

1.10.2 EKF and echosonar usage

1.10.3 Sensors in AUV

1.11 Thesis outline

Chapter 2
Chapter 3
Chapter 4
Chapter ??
Chapter ??
Chapter ??
Chapter 5

Chapter 2

Background

This chapter provides the theoretical background required to understand the subsequent developments of this work. It begins by introducing the conventions used to define reference frames in marine robotics, which form the basis for describing the general kinematic and dynamic equations of marine vehicles in six degrees of freedom (6-DOF) Fossen (2011).

The discussion then focuses on the critical role of sensors in marine robotics, with particular emphasis on their importance for autonomous navigation. The main challenges related to navigation sensing are outlined, and the key sensors used to implement the guidance and navigation systems are examined.
The analysis is limited to navigation-related sensors, specifically the AHRS, the DVL, and the echosounder, while auxiliary sensors for system monitoring and diagnostics are not considered. For each of the selected sensors, the chapter examines their role, the physical principles underlying their operation, and the potential issues that may arise during use.

Finally, the chapter provides a detailed description of the BlueRov2 in its heavy configuration. The dynamic model and its parameters are presented, based on an identification study conducted by the Dynamical Systems and Ocean Robotics group (DSOR) at the Instituto de Sistemas e Robótica, Instituto Superior Técnico (ISR-IST). The chapter concludes with an overview of the commercially available sensors integrated into the BlueRov2, highlighting key considerations and requirements for their correct installation and operation on the vehicle.

2.1 Dynamics of underwater vehicles

The study begins with the fundamental equation for underwater dynamics. The simplifications due to low-speed conditions, together with the most relevant parameters, will be illustrated in detail.

2.1.1 Reference frames and naming conventions

To tackle the study of AUV dynamics, it is essential to define the main reference frames in accordance with marine robotics conventions, namely the body-fixed frame, where the dynamic of the vehicle is described, and an earth-fixed frame, with respect to the position and the orientation of the vehicle are described.

The body-fixed frame $\{B\}$ is a right-handed coordinate system, it is rigidly attached to the vehicle, with its origin O_B located at the center of gravity (CG). The axes $\{x_B, y_B, z_B\}$ are defined following the "SNAME" notation The Society of Naval Architects and Marine Engineers (SNAME) (1950), so:

- the x_B axis points towards the head of the vehicle (longitudinal axis);
- the y_B axis points to the right side of the vehicle (transverse axis);
- the z_B axis points downwards (normal axis).

Having defined the robot's frame of reference, we now need to define a fixed observation reference to estimate the position and movement of the AUV. We can therefore assume the rotation and curvature of the Earth as zero, given the low-speed and small variations in latitude and longitude operating conditions. Based on these considerations, we define a earth-fixed-frame $\{I\}$ at a point on the sea surface within the vehicle's area of operation. Following convention, the frame will be a local NED (North-East-Down) frame, then a right-handed coordinate system, with the axes pointing respectively:

- the x_I axis pointing towards the North;
- the y_I axis pointing towards the East;
- the z_I axis pointing downwards.

Given the assumption stated earlier, $\{I\}$ can be considered an inertial frame, so Newton's laws of motion are valid.

Having defined the two reference frames, it is possible to introduce the SNAME notation for all parameters essential for determining the position, orientation and velocity of the AUV, considering external forces and moments applied to it. The position of the origin of the body-fixed frame with respect to the inertial frame is defined through the vector $\eta_1 = [x, y, z]^T$, while the orientation of $\{B\}$ with respect to $\{I\}$ is given by the rotation matrix ${}^I_B R$ defined by the Euler angles contained in the vector $\eta_2 = [\phi, \theta, \psi]^T$. The orientation of the vehicle is described by a sequence of intrinsic rotations following the Tait-Bryan convention (Z-Y'-X"). The velocity of $\{B\}$ with respect to $\{I\}$, on the other hand, is divided into linear $\nu_1 = [u, v, w]^T$ and angular $\nu_2 = [p, q, r]^T$ components, while the external forces

and moments are expressed in $\{B\}$ and are described by the vector $\tau = [\tau_1, \tau_2]^T$, where $\tau_1 = [X, Y, Z]^T$ for forces and by the vector $\tau_2 = [K, M, N]^T$ for moments.

This notation is more easily visible in the table 2.1, where the parameters that will be widely used in this thesis are defined in the 6 degrees of freedom.

DOF	Direction	Position and Euler angles	Velocity	Force and Moment
1	along x_B	x	surge speed u	X
2	along y_B	y	sway speed v	Y
3	along z_B	z	heave speed w	Z
4	rotation about x_B	roll angle ϕ	roll rate p	K
5	rotation about y_B	pitch angle θ	pitch rate q	M
6	rotation about z_B	yaw angle ψ	yaw rate r	N

Table 2.1: SNAME nomenclature and symbols Abreu (2014).

2.1.2 Kinematics

Kinematics equation describe the motion of the vehicle without considering the forces and moments that cause it. The kinematic equations relate the time derivatives of the position and orientation of the vehicle in the inertial frame to the linear and angular velocities in the body-fixed frame. To transform the velocities from the body-fixed frame to the inertial frame, we use the rotation matrix ${}^I_B R(\eta_2)$.

Using the rotation matrix, the kinematic equations can be expressed as:

$$\dot{\eta_1} = {}^I_B R(\eta_2)\nu_1 \tag{2.1}$$

the cartesian velocity in the inertial frame is obtained by multiplying the linear velocity in the body-fixed frame by the rotation matrix.

For the kinematic equations related to the angular velocity, the relationship is given by:

$$\dot{\eta_2} = \begin{bmatrix} 1 & sin(\phi)tan(\theta) & cos(\phi)tan(\theta) \\ 0 & cos(\phi) & -sin(\phi) \\ 0 & sin(\phi)/cos(\theta) & cos(\phi)/cos(\theta) \end{bmatrix} \nu_2 \iff \dot{\eta_2} = T(\eta_2)\nu_2 \tag{2.2}$$

where the matrix T relates the time derivatives of the Euler angles to the angular velocities in the body-fixed frame. Possible issues with singularities when $\theta = \pm 90°$ are not considered here, as they are not relevant for the application discussed in this thesis. When the terrain has a pitch inclination bigger than 80°, the AUV is no longer able to follow it and the AUV computer start the obstacle avoidance behavior.

All the details about derivation of this matrix and singularity issues can be found in Fossen (2011).

Finally combining equations 2.1 and 2.2, the complete kinematic equations can be expressed wih Jacobian terms, as:

$$\begin{bmatrix} \dot{\eta_1} \\ \dot{\eta_2} \end{bmatrix} = \begin{bmatrix} {}^I_B R(\eta_2) & 0_{3\times3} \\ 0_{3\times3} & T(\eta_2) \end{bmatrix} \begin{bmatrix} \nu_1 \\ \nu_2 \end{bmatrix} \iff \dot{\eta} = J(\eta)\nu \tag{2.3}$$

The kinematic equations will be used to obtain position and velocity information, integrating it with information from the sensors and filtering it to obtain a less noisy estimate of the state, as we will see in the chapter 3.

2.1.3 Dynamics

The dynamic equations of motion describe how forces and torques affect the movement of the vehicle. These equations are commonly expressed in the body-fixed reference frame, as this formulation keeps the inertia tensor constant and allows external forces (weight, buoyancy, hydrodynamic effects) to be represented more conveniently.

The derivation of the rigid-body dynamics follows Newton-Euler laws for both translational and rotational motion Fossen (2011):

$$\begin{cases} \sum F_{RB} = m[\nu_2 \times \nu_1 + \dot{\nu}_1] \\ \sum N_{RB} = I_{RB}\dot{\nu}_2 + \nu_2 \times I_{RB}\nu_2 \end{cases} \tag{2.4}$$

where m is the mass of the vehicle, I_{RB} is the inertia tensor, $\sum F_{RB}$ are the external forces and $\sum N_{RB}$ are the external moments acting on the vehicle.
The equations 2.4 can be rewritten in a more compact matrix form as:

$$M_{RB}\dot{\nu} + C_{RB}(\nu)\nu = \tau \tag{2.5}$$

M_{RB} is the rigid body inertia matrix, while C_{RB} contains the Coriolis and centrifugal terms. These matrices satisfy some key properties:

- $\dot{M}_{RB} = 0$: the inertia matrix is constant in the body-fixed frame;
- $\dot{M}^T_{RB} = \dot{M}_{RB}$: the inertia matrix is symmetric and positive-definite. Moreover, when the body-fixed frame is centered at the center of gravity and aligned with the principal axes of inertia, M_{RB} is diagonal;
- $C_{RB}(\nu) = -C_{RB}(\nu)^T$: the Coriolis and centripetal matrix can be parameterized to be skew-symmetric.

In this case, with the body-fixed frame centered at the center of gravity, the inertia matrix and the Coriolis matrix correspond to:

$$M_{RB} = diag(m, m, m, I_x, I_y, I_z) \qquad C_{RB}(\nu) = \begin{bmatrix} mS(\nu_2) & 0_{3\times3} \\ 0_{3\times3} & -S(I_{RB}\nu_2) \end{bmatrix} \tag{2.6}$$

where I_x, I_y, I_z are the moments of inertia about the principal axes, and $S(\cdot)$ is the skew-symmetric operator.
The subscript RB highlights that the formulation includes only rigid-body dynamics, with all external forces and moments grouped in the generalized vector $\tau_{RB} = [X, Y, Z, K, M, N]^T$. In order to account for different contributions, this term can be decomposed as:

$$\tau_{RB} = \tau + \tau_A + \tau_D + \tau_R + \tau_{dist} \tag{2.7}$$

where:

- τ represents control inputs given by the thrusters;
- τ_A accounts for added mass and added Coriolis effects, described by the matrices M_A and $C_A(\nu)$ respectively.

  $$M_A = -diag(X_{\dot{u}}, Y_{\dot{v}}, Z_{\dot{w}}, K_{\dot{p}}, M_{\dot{q}}, N_{\dot{r}}) \quad C_A(\nu) = \begin{bmatrix} 0_{3\times3} & -S(M_A\nu_1) \\ -S(M_A\nu_1) & -S(M_A\nu_2) \end{bmatrix} \tag{2.8}$$

  It can be studied by computing the kinetic energy imparted by the vehicle to the surrounding displaced fluid (even for inviscid fluid);
- τ_D models drag forces and moments, can be represented by inverting the sign with $D(\nu) = D_1 + D_2(\nu)$, where D_1 is a linear damping matrix, while $D_2(\nu)$ is a quadratic damping matrix. These terms account for hydrodynamic resistance, including contributions from skin friction and pressure-induced drag;
- τ_R represents restoring forces and moments arising from buoyancy and weight imbalance. Defining $\mathbf{r}_b = [x_b, y_b, z_b]^T$ as the position vector of the center of buoyancy (CB) relative to the origin of the body frame and having the origin of $\{B\}$ at the CG, the restoring forces and moments can be expressed as:

  $$\mathbf{g}_\eta = \begin{bmatrix} {}^I_B R^T(\eta)\,[0, 0, W - B]^T \\ -r_b \times {}^I_B R^T(\eta_2)\,[0, 0, B]^T \end{bmatrix}. \tag{2.9}$$

  Here, W is the weight of the vehicle, $B = \rho_{seawater} g V$ is the buoyant force (V is the volume discplacement of the AUV), and ${}^I_B R(\eta_2)$ is the rotation matrix from the body-fixed frame to the inertial frame.

- τ_{dist} includes unmodeled external disturbances such as waves (not important in my application) and currents.

So, the equation 2.5 can be rewritten as:

$$\tau_{RB} = \tau - M_A\dot{\nu} - C_A(\nu)\nu - D(\nu)\nu - \mathbf{g}(\eta) + \tau_{dist} \tag{2.10}$$

The complete dynamic model, neglecting the disturbances, becomes:

$$(M_{RB} + M_A)\dot{\nu} + (C_{RB}(\nu) + C_A(\nu))\nu + D(\nu)\nu + \mathbf{g}(\eta) = \tau, \tag{2.11}$$

Or more compactly:

$$M\dot{\nu} + C(\nu)\nu + D(\nu)\nu + \mathbf{g}(\eta) = \tau, \tag{2.12}$$

By assuming that the origin of the body-fixed reference frame coincides with the vehicle's center of gravity, that the body axes are aligned with the principal axes of inertia, that the added mass matrix M_A is symmetric and positive definite, and that hydrostatic stability conditions hold, then the overall inertia matrix M is symmetric and positive definite. Furthermore, the damping matrix $D(\nu)$ is positive definite, while the Coriolis-centripetal matrix $C(\nu)$ can be parameterized to be skew-symmetric.
When the matrix form of the dynamic model is expanded, it yields the full set of equations corresponding to the six degrees of freedom:

$$\begin{aligned}
m_u\dot{u} - m_v vr + m_w wq + d_u u &= \tau_u \\
m_v\dot{v} + m_u ur + m_w wp + d_v v &= \tau_v \\
m_w\dot{w} - m_u uq + m_v vp + d_w w &= \tau_w \\
m_p\dot{p} - m_{vw} vw - m_{qr} qr + d_p p + z_b B cos(\theta) sin(\phi) &= \tau_p \\
m_q\dot{q} + m_{uw} uw + m_{pr} pr + d_q q - z_b B sin(\theta) &= \tau_q \\
m_r\dot{r} - m_{uv} uv - m_{pq} pq + d_r r &= \tau_r
\end{aligned} \tag{2.13}$$

Where the following parameters are defined:

$$\begin{aligned}
m_u &= m - X_{\dot{u}} & m_{uv} &= m_u - m_v & d_u &= -X_u - X_{|u|u}|u| \\
m_v &= m - Y_{\dot{v}} & m_{uw} &= m_u - m_w & d_v &= -Y_v - Y_{|v|v}|v| \\
m_w &= m - Z_{\dot{w}} & m_{vw} &= m_v - m_w & d_w &= -Z_w - Z_{|w|w}|w| \\
m_p &= I_x - K_{\dot{p}} & m_{pq} &= m_p - m_q & d_p &= -K_p - K_{|p|p}|p| \\
m_r &= I_y - M_{\dot{q}} & m_{pr} &= m_p - m_r & d_q &= -M_q - M_{|q|q}|q| \\
m_r &= I_z - N_{\dot{r}} & m_{qr} &= m_q - m_r & d_r &= -N_r - N_{|r|r}|r|
\end{aligned}$$

2.2 Sensors

Sensory systems are fundamental to the autonomous operation of Autonomous Underwater Vehicles (AUVs), enabling precise navigation, mapping of the marine environment, and acquisition of scientific data in underwater operating conditions. The underwater environment presents unique challenges for sensors, including the absence of beacons and GPS signals, attenuation of electromagnetic communications, and poor visibility conditions. Moreover, the unknown environment doesn't allow for the use of pre-existing maps, making real-time perception and navigation essential.

2.2.1 Sensors for dead reckoning

The sensor configuration for autonomous navigation of a modern AUV typically integrates four main sensors: pressure sensor, attitude and heading reference systems (AHRS), Doppler velocity measurement systems (DVL), and echosounder arrays for seabed scanning (or a camera). This sensory combination provides the depth of the AUV estimation, the capabilities for inertial navigation, the estimation of the vehicle's velocity relative to the inertial reference frame, and surrounding environment perception capabilities necessary for autonomous underwater operation. Each sensor requires sophisticated data fusion algorithms, such as the Kalman Filter (addressed in 3), to reduce the inherent noise and errors in their measurements. Moreover, in many cases, it is necessary to combine information from different sensor sources, compensating for the individual limitations of each system and improving the overall accuracy of navigation and environmental perception. Indeed, when for a long time the AUV does not receive his absolute position, the error in the position estimate tends to grow unbounded, a phenomenon known as drift. One simple solution, but not the most accurate, is to fuse the AHRS and DVL data to estimate the AUV's position through dead reckoning.

2.2.2 Attitude and heading reference system

The Attitude and Heading Reference System (AHRS) is a key sensor for determining the orientation of the AUV in three-dimensional space. It typically fuses data from three types of Micro-Electro-Mechanical Systems (MEMS) to provide accurate estimates of roll, pitch, and yaw angles.
Other AHRS technologies exist, such as Fiber Optic Gyroscopes (FOG) or Ring Laser Gyroscopes (RLG), which offer higher precision but are more expensive and primarily used in specialized applications. MEMS technology, being standard for the BlueRov2, will be the focus here.
These MEMS-based AHRS typically include Klūga *et al.* (2024):

- Triaxial gyroscope: Measures angular velocities around the three axes, capturing rapid changes in orientation.
- Triaxial accelerometer: Measures linear accelerations along the three axes, which can be used to estimate roll and pitch angles.
- Triaxial magnetometer: Measures the magnetic field strength along the three axes, providing heading information relative to the Earth's magnetic field.

The physical principles of these sensors differ. The gyroscope uses the Coriolis effect to measure the motion of internal proof masses proportional to the angular velocity; however, it is prone to drift over time due to temperature variations and aging, and it cannot provide absolute orientation or heading information. The accelerometer relies on Newton's second law of motion to measure linear acceleration by sensing the direction of gravity, but its readings can be affected by dynamic accelerations. The magnetometer used in the BlueRov2 is an Anisotropic Magneto-Resistance (AMR) sensor, which exploits the tendency of certain materials (typically ferromagnetic) to change their electrical resistance in response to the Earth's magnetic field. However, it is more susceptible to noise induced by the AUV's structure. The magnetic field measurement's bias is hard to estimate Troni & Eustice (2014) because the bias interface depend on the environmental aspect, which are varying both with time and space in all directions, therefore it requires careful calibration and filtering Ko *et al.* (2016a).
The AHRS combines the data from these three sensors using sensor fusion algorithms, such as the Extended Kalman Filter (EKF) or complementary filters, to provide a robust and accurate estimate of the AUV's orientation. The gyroscope data is used for short-term orientation changes, while the accelerometer and magnetometer data are used to correct for drift and provide absolute orientation references. The roll and pitch angles are primarily derived from the accelerometer readings, which are generally more reliable than the magnetometer data.
The acquisition of the yaw angle depends primarily on the magnetometer readings. Consequently, due to noise, the yaw estimate is generally less accurate than the roll and pitch angles Ko *et al.* (2016b). In this work, this is not a major issue because the yaw angle is mainly relevant for the path-following node and not for the terrain-following node. However, it is still actuated to generate a simple trajectory to test the algorithm performance.
To improve the reliability of the heading, it is often necessary to fuse the AHRS data with the DVL measurements to obtain a more accurate yaw angle estimation. For completeness, it is worth noting that more precise magnetometers, such as Fluxgate sensors, exist but are also significantly more expensive and may not always fit within the AUV's design constraints Timmermann *et al.* (2025).

AHRS measurements are typically provided at frequencies ranging from 50 to 200 Hz, delivering real-time orientation data to the AUV's control system. The optimal sampling frequency is generally between $200Hz$ and $400Hz$, with a bandwidth of $10Hz$ to $50Hz$, to ensure reliable acquisition at the AUV's operating rate.

The AHRS is essential for stabilizing vehicle motion and achieving precise navigation, but its integration in an AUV requires specific considerations. It should be mounted near the AUV's center of gravity to minimize the influence of dynamic linear accelerations and isolated from vibrations and shocks that could degrade sensor readings.

2.2.3 Doppler Velocity Log (DVL)

The Doppler Velocity Log (DVL) is a crucial sensor for measuring the relative velocity of an AUV. It relies on the Doppler effect, which occurs when the frequency of a wave appears altered due to the relative movement between the source emitting the wave and the observer receiving it. In fact, the DVL transmits acoustic pulses along multiple beams, directed in different directions, and measures the frequency shift of the echoes reflected by the receivers. By analyzing these frequency shifts, the DVL can calculate the velocity of the AUV, relative to the receiver, following this formula:

$$\Delta f = \frac{2 f_0 v cos(\theta)}{c} \tag{2.14}$$

where Δf is the frequency shift, f_0 is the emitted frequency, v is the three dimensional relative velocity of the AUV, θ is the angle between the acoustic beam and the direction of motion, and c is the speed of sound in water Annapurna *et al.* (2024).

This device, mounted in the underside of the AUV, usually employs four acoustic beams in a Janus configuration, which allows for the measurement of velocity in three dimensions. Each beam is oriented at a specific angle to the vertical axes, typically around 20 to 30 degrees, to measure:

- Forward and backward velocity components (surge)
- Lateral velocity components (sway)
- Vertical velocity components (heave)

Considering the formula 2.14 we can focus on three main factors that influence the DVL performance. The speed of the sound in water c is affected by environmental conditions such as temperature, salinity, and pressure. This variability can introduce errors in velocity measurements if not properly compensated. The angle θ

of the acoustic beams is critical for accurate velocity estimation. Misalignment or calibration errors can lead to significant inaccuracies, especially in the lateral and vertical velocity components. In the end the emitted frequency f_0 also plays a role, as higher frequencies provide better resolution but are more susceptible to attenuation in water, limiting the effective range of the DVL. instead, lower frequencies can travel further but may offer less precise measurements. There are different frequency choices for DVLs, like $600kHz$ for short-range and high accuracy applications, or 38 kHz for long-range applications with lower accuracy Sarangapani (2022).

There are two operating modes of DVL: the bottom-tracking mode (DVL-bt) and the water-tracking mode (DVL-wt). The bottom-tracking mode measures the velocity of the AUV relative to the seabed. The accuracy of the data depends also on the seabed material composition and geometry, as soft sediments can absorb acoustic signals, or some acoustic beams may be lost, leading to weaker echoes and less reliable velocity measurements. However, When operating in mid-water zone, the DVL may lose bottom track due to the limited sensor range. In this case, its measurements will be affected by sea currents Liu *et al.* (2022). This is the water-tracking mode, which measures the velocity relative to the water mass, knowing that $v_{water} = v_{AUV} - v_{current}$.
It is possible thanks to the presence of small particles or plankton in the water that reflect the acoustic signals, but only using high frequencies. However, this mode is generally less accurate than bottom-tracking, as the water mass can have its own movement due to currents, which estimation is not always available.

The main issue with DVLs is the partial or complete outage of the sensor, where some or all four beams are missing and the DVL is not able to provide the velocity update Cohen *et al.* (2022). To solve this issue different techniques exist, like the integration with AHRS data and the Kalman filter or deep learning algorithms, as Yampolsky *et al.* (2025).

2.2.4 Echosounder

The echosounder is a fundamental sensor for underwater terrain detection and mapping. It operates by emitting acoustic pulses into the water and measuring the time-of-flight of the echoes reflected from the seabed or other underwater objects, so the time taken for the sound wave to travel to the target and back. This time measurement is then used to calculate the distance to the target using the speed of sound in water, considering the simplified equation:

$$d = \frac{c \cdot t}{2} \tag{2.15}$$

where d is the distance to the target, c is the speed of sound in water, and t is the measured time-of-flight. The division by 2 accounts for the round trip of the acoustic signal. To generate the sound waves, the echosounder uses a piezo-electric transducer that converts electrical energy into acoustic energy and vice versa when the wave is reflected back. Obviously there are different materials and designs for the transducer, which can affect the performance of the echosounder in terms of range, resolution, and beamwidth. The echosounder can operate in different modes, such as single-beam or multi-beam configurations. Single-beam echosounders (SBES) emit a single acoustic pulse and measure the distance directly below the AUV, while multi-beam echosounders (MBES) emit multiple beams in a fan-shaped pattern, allowing for a wider area coverage and more detailed mapping of the seabed. For my AUV application i will use 4 SBES, mounted in a cross configuration to estimate the inclination angle of the seabed in roll and pitch. This solution is a compromise between cost, complexity, and performance, as MBES are generally more expensive and require more processing power to handle the larger amount of data generated, that in this case is not needed. The choice of frequency for the echosounder is also crucial, as higher frequencies provide better resolution but are more susceptible to attenuation in water, limiting the effective range of distance of the sensor. The frequency in industrial SBES run from 12 KHz to 400KHz, with lower frequencies being used for deep-water applications and higher frequencies for applications close to the seabed.

To estimate the seabed inclination other technologies exist, such as the laser scanner or the stereo camera, but they requires specific conditions to operate, like good visibility and low turbidity, which are not always guaranteed in unknown underwater environments. They are also more expensive than the single beam echosounder. The laser scanner requires the AUV close to the seabed (less than 2m of distance for laser standard technology) to obtain accurate measurements, while the stereo camera relies on sufficient lighting and texture in the environment to function properly.

2.3 BlueRov2 AUV

The BlueROV2 is a commercial ROV (Remotely Operated Vehicle) developed by Blue Robotics. It is an open-source, modular system that is widely used in both academic and industrial settings for research, testing, and inspection applications. Its frame is built from high-strength anodized aluminum and plastic components, ensuring durability while keeping the overall weight, 11.5 Kg, light. The open-frame structure allows easy integration of additional sensors, payloads, and modifications.

Having the “heavy configuration“ kit for the BlueRov2, the vehicle is equipped

with eight thrusters (Blue Robotics T200) arranged in a vectored configuration. Four thrusters are mounted on the horizontal plane, oriented at 45° with respect to the vehicle axes, allowing precise control of surge, sway, and yaw. The other four thrusters are mounted vertically, enabling heave, pitch, and roll control. This configuration provides actuation over all six degrees of freedom, making the BlueROV2 a fully actuated underwater vehicle.

The vehicle's buoyancy and stability are provided by syntactic foam blocks mounted on the upper part of the frame, while ballast weights are attached at the bottom to lower the center of gravity. Knowing the mass of the vehicle, the volume $V = 0.011054$, the density of water $\rho_{seawater} = 1028$ and $r_b = [0, 0, 0.0420]^T$, we can easily compute the restoring component.

Further technical details about the BlueROV2 and its components can be found in the official datasheets provided by the manufacturer BlueRov2 datasheet and thrusters T200 datasheet.
motivo....

The coefficients of the BlueRov2 model used are derived from the identification work carried out by DSOR-ISR, they are described in the following 2.2:

Inertia	Added mass	Linear damping	Quadratic Damping
$I_x = 0.21$	$X_{\dot{u}} = -27.08$	$X_u = -0.1213$	$X_{\|u\|u} = -23.9000$
	$Y_{\dot{v}} = -25.952$	$Y_v = -1.1732$	$Y_{\|v\|v} = -46.2700$
$I_y = 0.245$	$Z_{\dot{w}} = -29.9081$	$Z_w = -1.1130$	$Z_{\|w\|w} = -50.2780$
	$K_{\dot{p}} = -1$	$K_p = -0.5$	$K_{\|p\|p} = -1$
$I_z = 0.245$	$M_{\dot{q}} = -1$	$M_q = -0.5$	$M_{\|q\|q} = -1$
	$N_{\dot{r}} = -1$	$N_r = -0.5$	$N_{\|r\|r} = -1$

Table 2.2: Added mass, linear damping and quadratic damping coefficients of the BlueRov2 robot

It is valuable to be aware that these parameters are coefficients that best represent the dynamic model of BleuRov2, but they involve an error in the estimation of the state that can be compensated for by using specific sensors in the underwater robot.

Although the BlueROV2 is originally designed as a Remotely Operated Vehicle (ROV), in this work it is modeled and employed as an Autonomous Underwater Vehicle (AUV). This choice is justified by the fact that the platform is fully actuated in all six degrees of freedom, with independent thrusters for each motion, making it a suitable candidate for testing the proposed control and estimation algorithms in simulation. The BlueROV2's open-source nature and modular design allow for easy integration of additional sensors and payloads. Futhermore, even if

the wire is not used, it can be used to easily retrieve the robot from the seabed, either manually or remotely during initial sea trials. In the following sections, the BlueROV2 will therefore be analyzed as an AUV, even though it is not one in practice. The possible hardware and software modifications required to achieve such a transformation in reality are beyond the scope of this work and will not be addressed, but one possible discussion in detail can be found in Willners *et al.* (2021).

Chapter 3

Methodology

Tutto ciò che ho studiato e sviluppato durante la tesi va descritto in questo capitolo. KF, EKF, PID eccetera.

Chapter 4

Software Architecture

Scrivere architettura software e le integrazioni tra i diversi programmi

Chapter 5

Results and Simulations

Write the results here...

Chapter 6

Conclusions

Write the conclusions here...

Appendix A

Extra

Write here...

Write here...

References

Abreu, P.C. (2014). Sensor-based Formation Control of Autonomous Underwater Vehicles. 8

Annapurna, S.M., Sarath Chandran, R., Haneesh Sankar, T.P. & Rajesh, K.R. (2024). Enhancing Accuracy in Doppler Frequency Shift Estimation and Velocity Measurement for Doppler Velocity Log Applications: A Comparative Study. In *2024 11th International Conference on Signal Processing and Integrated Networks (SPIN)*, 322–327. 14

Caccia, M., Bruzzone, G. & Veruggio, G. (1999). Active sonar-based bottom-following for unmanned underwater vehicles. *Control Engineering Practice*, **7**, 459–468. 1

Cohen, N., Yampolsky, Z. & Klein, I. (2022). Set-Transformer BeamsNet for AUV Velocity Forecasting in Complete DVL Outage Scenarios. 15

Eliav, J. (2015). Guglielmo's Secret: The Enigma of the First Diving Bell Used in Underwater Archaeology. *The International Journal for the History of Engineering & Technology*, **85**, 60–69. 4

Erodoto (V sec. a.C.). Storie. 4

Fossen, T.I. (2011). *Handbook of Marine Craft Hydrodynamics and Motion Control*. Wiley, 1st edn. 6, 9

Jacques Piccard, R.S.D. (1961). Seven Miles Down. 4

Klūga, J., Grabs, E., Chen, T., Ancāns, A., Stetjuha, M., Rjazanovs, D. & Ipatovs, A. (2024). Motion Sensors Data Fusion for Accurate Measurement in AHRS Systems. In *2024 Photonics & Electromagnetics Research Symposium (PIERS)*, 1–4, IEEE, Chengdu, China. 12

Ko, N., Jeong, S. & Bae, Y. (2016a). Sine Rotation Vector Method for Attitude Estimation of an Underwater Robot. *Sensors*, **16**, 1213. 13

Ko, N.Y., Jeong, S., Choi, H.T. & Moon, Y.S. (2016b). Comparison of Attitude Estimation Methods for Underwater Navigation. *International Journal of Mechanical Engineering and Robotics Research*, **7**, 285–291. 13

Liu, P., Wang, B., Li, G., Hou, D., Zhu, Z. & Wang, Z. (2022). SINS/DVL Integrated Navigation Method With Current Compensation Using RBF Neural Network. *IEEE Sensors Journal*, **22**, 14366–14377. 15

Sarangapani, S. (2022). Multi-frequency Phased Array Transducer for ADCP Applications. In *OCEANS 2022 - Chennai*, 1–10. 15

The Society of Naval Architects and Marine Engineers (SNAME) (1950). Nomenclature for treating the motion of a submerged body through a fluid. 7

Timmermann, G., Pöppelwerth, A., Richter, I., Auster, H.U. & Plaschke, F. (2025). Comparison of noise levels of different magnetometer types and space environments. 13

Troni, G. & Eustice, R.M. (2014). Magnetometer bias calibration based on relative angular position: Theory and experimental comparative evaluation. In *2014 IEEE/RSJ International Conference on Intelligent Robots and Systems*, 444–450. 13

Willners, J.S., Carlucho, I., Łuczyński, T., Katagiri, S., Lemoine, C., Roe, J., Stephens, D., Xu, S., Carreno, Y., Pairet, È., Barbalata, C., Petillot, Y. & Wang, S. (2021). From market-ready ROVs to low-cost AUVs. 18

Yampolsky, Z., Cohen, N. & Klein, I. (2025). Transformer-Based Robust Underwater Inertial Navigation in Prolonged Doppler Velocity Log Outages. 15